The Actuator With Mechanically Adjustable Series Compliance

Jonathan W. Hurst, Joel E. Chestnutt, and Alfred A. Rizzi

***Abstract*—Running is a complex dynamic task that places strict requirements on both the physical components and software-control systems of a robot. This paper explores some of those requirements and, in particular, explores how a variable-compliance actuation system can satisfy many of them. We present the mechanical design and software-control system for such an actuator system. We analyze its performance through simulation and bench-top experimental validation of a prototype version. In conclusion, we demonstrate, through simulation, the application of our proof-of-concept actuator to the problem of biped running.**

***Index Terms*—Actuators, force control, legged locomotion, natural dynamics.**

I. Introduction

A ROBOT designed specifically for autonomous legged locomotion should be capable of highly dynamic running, jumping, and stumble recovery and should achieve these capabilities while being energetically efficient. In order to accomplish these goals, we believe a leg spring of sufficient capacity to store the energy of a running gait is virtually a necessity. Furthermore, we believe variable leg stiffness provides an important means for effective gait control.

There are two extremes of actuator design that might achieve the desired capabilities: software control of all dynamic properties or careful design of a mechanical system to passively exhibit a desired behavior. The first approach is more flexible, and such an actuator could exhibit many different behaviors; however, there are strict limitations imposed by current actuator technology. The second approach can exhibit only a single behavior, such as hopping, but perhaps much more effectively than the first approach.

The actuator with mechanically adjustable series compliance (AMASC), as shown in Fig. 1, represents a carefully chosen balance between the two design extremes. The natural dynamics of the system are engineered and utilized, where possible, to maximize performance, while the software-control system adds energy that is lost in the mechanism, and creates behaviors that are not inherent in the natural dynamics. Actuators based on this proof of concept can be used to implement the spring-loaded inverted pendulum (SLIP), shown in Fig. 2 [1]–[3]. In addition to its potential utility in legged locomotion, mechanically adjustable stiffness is important for general-purpose actuation, because the optimal stiffness will change for different tasks such as reaching motions, object manipulation, force control, and safety in human–robot physical interaction [4]. We aim to sufficiently convince the reader that several ideas implemented in the AMASC could be valuable methods for designing variable-compliance mechanisms. We demonstrate a functioning prototype, and show that a very simple mathematical model represents the dynamics of the relatively complex device. This archival journal paper adds detailed information to the published conference paper about the AMASC [5].

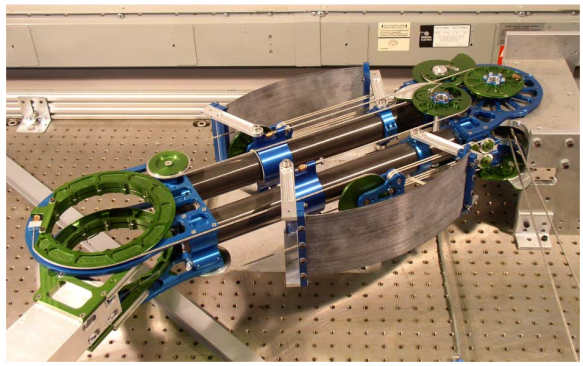

Fig. 1. The actuator with the mechanically adjustable series compliance (AMASC).

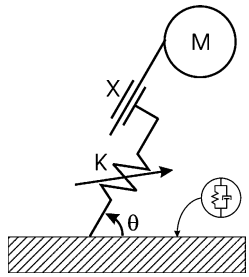

Fig. 2. The SLIP model of running can be controlled by manipulation of three variables: a spring constant K, spring rest length x, and touchdown angle θ.

Manuscript received October 11, 2009; revised April 30, 2010; accepted June 2, 2010. Date of publication July 8, 2010; date of current version August 10, 2010. This paper was recommended for publication by Associate Editor K. Hosoda and Editor G. Oriolo upon evaluation of the reviewers' comments. This work was supported in part by a National Science Foundation Graduate Fellowship held by J. W. Hurst and by the Robotics Institute of Carnegie Mellon University. This paper was presented in part at the IEEE International Conference on Robotics and Automation, New Orleans, LA, 2004.

J. W. Hurst is with the School of Mechanical, Industrial, and Manufacturing Engineering, Oregon State University, Corvallis, OR 97331-6001 USA (e-mail: jonathan.hurst@oregonstate.edu).

J. E. Chestnutt is with the Digital Human Research Center, National Institute of Advanced Industrial Science and Technology, 135-0064 Tokyo, Japan (e-mail: joel.chestnutt@aist.go.jp).

A. A. Rizzi is with Boston Dynamics, Inc., Boston, MA 02451-7507 USA (e-mail: arizzi@bostondynamics.com).

Color versions of one or more of the figures in this paper are available online at http://ieeexplore.ieee.org.

Digital Object Identifier 10.1109/TRO.2010.2052398

II. Background

Most research papers that analyze the mechanics of running base this analysis on some form of the SLIP model, as shown in Fig. 2. This model can be used to describe the motion of the center of mass of a running animal [6], [7] or a running robot. The basic definition of running [8] is linked to the SLIP idea—energy is transferred from kinetic and gravitational potential energy in the flight phase to spring energy in the stance phase, and *vice versa*.

A. Compliance and Running

Physical series compliance is virtually necessary to achieve a robust, energetically economic running gait. Simulating compliance using a rigid actuator, such as an electric gearmotor, is not practical for three reasons: bandwidth limitations, power-output limitations, and energetic efficiency. For a realistic example, imagine a pogo stick that uses a gearmotor, power electronics, and batteries in place of the coil spring. To achieve the power output of the coil spring, a very large motor would be required, thereby adding significant weight to the pogo stick. If the power demands could be met, then the device would not last long before running out of batteries, because the electric system is much less efficient at storing and releasing energy than a mechanical spring.

The bandwidth limitation of an electric motor is due, in large part, to the high reflected inertia that is linked rigidly to the robot leg. Electric motors must be significantly geared to provide useful torque for robotics applications, and the reflected inertia of the rotor is amplified by the square of the gear reduction. The reflected inertia can be larger than the inertia of the entire robot, making a correct dynamic response to impacts impossible. Upon impact with the ground, the stationary motor instantaneously matches speed with the moving mass of the robot, thereby causing a large force spike and a loss of energy in the inelastic collision. Even with instantaneous sensing and computation, the torque required to accelerate the motor instantly to match the ground speed during an unexpected impact will exceed the motor's torque limit. Despite the drawbacks, some legged robots use this approach for running gaits, including Honda's Asimo [9]. We believe that the energetic economy and robustness to disturbances could be dramatically improved through the appropriate use of series compliance.

Passive series springs can alleviate many of the problems that are inherent in direct actuation schemes for locomotion. They can be used for energy storage, power transmission, or a combination of the two, as illustrated in Fig. 3. A physical spring has arbitrarily high power density, depending on its stiffness, but with bounded energy density. Motors and batteries have relatively low power density in comparison but have a much higher energy density per unit mass, thereby making a compelling argument for combining the two systems in a series combination. The spring can absorb and output energy at high power, while the motor can add and remove energy as needed, without handling all of the power transferred in a running gait.

Springs are particularly useful in rhythmic systems, because energy can be stored and released much more efficiently through

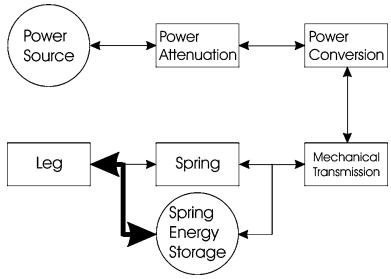

Fig. 3. In a series spring system, energy can be transmitted through the spring if it does not compress, or energy can be stored and released from the spring as it deflects. For a cyclic system, such as a running gait, most of the energy can be stored and returned with each stride, thereby eliminating the energy transfer and losses through the rest of the transmission.

a spring than if it were passed through the motor, transmission, and power electronics with each transfer. Not only do physical springs reduce wasted energy with each stride, but they also significantly reduce the necessary size and weight of many of the motor and transmission components. Minimizing weight reduces the total amount of energy that needs to be transferred with each stride. Animals make use of physical springs in their running gait, most likely for these reasons and more [10], [11].

B. Physically Variable Compliance as a Method of Control

While physical compliance is virtually a necessity for successful running, varying the compliance provides a useful tool for gait control. Research has shown that animals can adjust leg stiffness and vary it to control running and hopping in certain situations [12]–[14].

The normal steady-state motion of a SLIP-based running gait can be described by three parameters. In Schwind and Koditschek's mathematical analysis, leg length and angular velocity at the bottom of the stance, along with the leg stiffness, were chosen [1]. Control of forward speed, stance duration, and flight duration was demonstrated experimentally in Hodgins and Raibert's work with running robots [15]. Another choice might be leg stiffness, hopping height, and stride length; there are many possible three-variable parameterizations that could be considered. Because the SLIP model has only three terms available to control the three parameters of a running gait, the absence of one term may limit the control choices, and certain disturbances to the SLIP-model running gait may not be controllable. For example, if a SLIP runs over terrain that varies in stiffness, the leg stiffness must change or the running gait will be altered.

Most research suggests that animals prefer to maintain leg stiffness over a range of running speeds; however, they do change leg stiffness when other methods of control are not available [3], [16]–[18]. For example, hopping or running on a surface of changing stiffness [6], [12], [16], hopping in place with varying frequency [6], [12], or running at different speeds with constant stride length [17].

C. Actuator Design

Researchers at the Massachusetts Institute of Technology (MIT) did pioneering work in the field of compliant actuation with the development of the series elastic actuator (MIT-SEA)

[19]. Different implementations of the device used both electric and hydraulic power, with similar results. The MIT-SEA was developed as a force actuator for robot arms, and the design was later refined and used on several walking robots [20]–[23]. The springs on the MIT-SEA are essentially acting as a force sensor for the low-level controller, like a soft load cell.

Several mechanisms have been developed with variable series compliance, with varying configurations [24]. Some are designed for manufacturing or manipulation tasks involving constrained contact or impacts, which benefit from the high bandwidth of passive dynamics [25]–[29], while others are research platforms to explore biomimetic control of joint stiffness and position [30]–[32]. One drawback to most of these mechanisms is that they rely on two antagonistic motors, cocontracting nonlinear springs to change the stiffness of a driven joint. As in animals, this cocontraction uses energy, because the motors must apply force to compress the springs and hold a particular stiffness value. Some mechanisms use a leaf spring that is shortened or lengthened to adjust the stiffness, which avoids the energy inefficiency of antagonistic motors. Others rely on an adjustable mechanical advantage to change stiffness, but cannot control the stiffness function [33]. Most of these examples are designed for purposes other than legged locomotion and incorporate small springs that can store very little energy relative to that required of a running gait.

Pneumatic actuators are inherently springy and can store plenty of energy, which has led to their successful use on several running and hopping robots [34]. Pneumatic actuators used in antagonistic pairs have also been used to control the passive compliance of an actuated joint, thereby leading to moderate success in bipedal locomotion [35]. However, pneumatic actuators are also inherently difficult to control, energetically lossy, and difficult to power without an external compressor. Electrical actuation allows for much more precise control and allows for easier tether-free operation. For these reasons, we chose to use electric actuation, although the ideas presented in this paper could be implemented with some other form of actuation.

Mechanically adjustable series compliance may also be useful for control stability. Several researchers have shown that certain types of physical compliance are important for force control [36]–[38]; it is intuitive that a very low-stiffness joint is more capable of applying a constant force in the face of position disturbances than a rigid joint [4]. For good position control, higher stiffness improves disturbance rejection, and humans maximize their arm stiffness to hold a specific position. However, high stiffness combined with neural delay can lead to instabilities such as increased hand tremor [39]. Humans choose specific arm stiffnesses to stabilize different dynamic motions and to accommodate different reaching motions, likely choosing between disturbance rejection and control stability [40], [41].

III. Actuator With Mechanically Adjustable Series-Compliance Design

The natural dynamics of a system are an inseparable part of its behavior. The mechanical design, which determines the natural dynamics of a system, is thus an essential part of the overall control system design. The actuator presented here is an integrated mechanism and software controller, with mechanical design choices made to closely match the dynamic behavior of a simple, understandable, controllable mechanical model, as illustrated in Fig. 4. By designing the mechanism for this purpose, the control system is dramatically simplified over using a very complex mathematical model. Throughout the remainder of this paper, we will use the notational conventions of Table I.

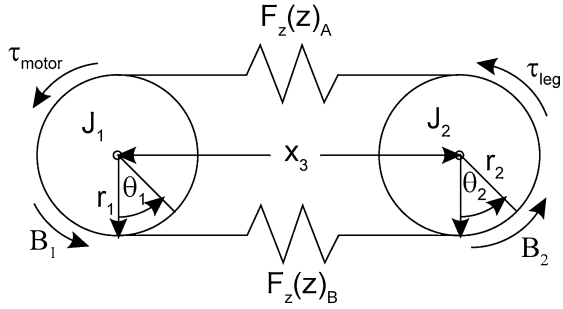

Fig. 4. Mechanical model of the physical actuator.

TABLE I
Definitions of Symbols Describing the AMASC

variable	description
θ_1	Motor position (rad)
θ_2	Leg position (rad)
r_1	Effective radius of motor pulley (m)
r_2	Effective radius of end effector pulley (m)
x_1	$\theta_1 \cdot r_1$, Motor position in cable length (m)
x_2	$\theta_2 \cdot r_2$, Leg position in cable length (m)
J_1	Motor inertia $(kg\text{-}m^2)$
J_2	Leg inertia $(kg\text{-}m^2)$
B_1	Rotor damping
B_2	Knee Damping
x_3	Pretension (m)
Δx	Linear leg deflection, $\theta_2 r_2 - \theta_1 r_1$ (m)
z	Deflection of the cable after the pulley function: $(x_3 + \Delta x)$ or $(x_3 - \Delta x)$ (m)
$F_{eff}(x_3, \Delta x)$	Knee force, τ_{eff}/r_2 (N)
$G(z)$	Spiral pulleys; spring position as a function of z (m)
y	Deflection of the spring, before the pulleys (m)
$F_y(y)$	Force function of the spring
$F_z(z)$	Force on the cable after the pulley function

The AMASC is essentially a single compliant joint, which most closely resembles a knee, endowed with engineered natural dynamics. There are two degrees of freedom with two corresponding motors. In addition, there are two identical opposing springs, much like antagonistic muscles in animals. One motor controls the spring pretension, thereby stretching both springs, which is represented by x_3 in Fig. 4. This degree of freedom is analogous to muscle cocontraction in animals. The knee joint does not move as a result of changes to x_3, but its rotational stiffness changes, thereby allowing the actuator to tune the stiffness of the natural dynamics. The other motor controls the spring rest position, θ_1, which is used as the primary energy source and controls any motions not described by the system's natural dynamics. These two motor-controlled parameters, along with the leg angle at touchdown, provide all three parameters for control of a SLIP-model robot.

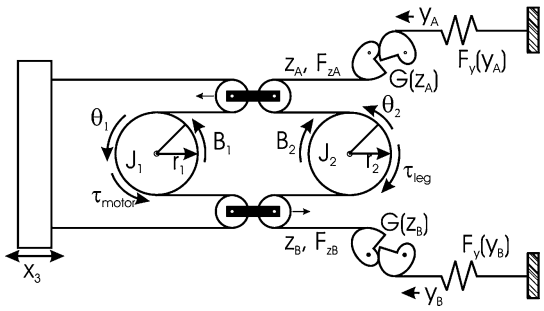

Fig. 5. Cable-routing diagram of the AMASC. J_1 and J_2 are pinned in place but can rotate freely; the spiral pulleys are also pinned in place but are free to rotate. The remaining four pulleys are floating and can move sideways as well as rotate. For notation descriptions, see Table I.

A. Mechanical Design

Many of the mechanism design challenges are common ones; for example, minimizing friction, backlash, mass, and inertia. Several specific choices were made that influence each of these attributes, such as the location and type of speed reduction, choice of materials, and type of motor. Minimizing mass was a concern throughout the design process, because the AMASC was intended as a prototype leg for a bipedal robot with approximately 1 m leg length and 30 kg total mass. Of this 30 kg, 20 kg is reserved for motors, batteries, and computing. This allotment leaves only 10 kg for the entire framework and mechanism, including springs and power transmission. To minimize weight, all joints contain thin-section bearings, which are very light for a given load rating. All parts are machined aluminum, with the main structural members (analogous to the femur) made of thin-wall aluminum tube. The mass of this actuator prototype is approximately 4 kg, and the dimensions are nearly 50% oversized.

In order to create a low-friction, zero-backlash system, the AMASC utilizes a high-speed cable drive [42]. There is some stretch in the cable transmission, which adds series compliance to the system and is incorporated into the effective spring constant of our model. Because the cables are round, they may wrap around pulleys placed at any angle, unlike standard belts. This design freedom makes it easier to route cables through joints, thereby allowing the motors to be located remotely. Fig. 5 shows a diagrammatical representation of the cable routing, which illustrates the role of each motor in the tension of the two springs. Also shown is the fact that a displacement of the leg, θ_2, results in displacement of the motor, θ_1, displacement of the springs, or some combination of the two. There is a speed reduction between the first and second pulleys, which is not shown on the diagram; it is implemented using a combination of a block-and-tackle pulley mechanism and a difference in radii between r_1 and r_2. The speed reduction is physically located near the knee joint, but diagrammatically located near the motor θ_1. In all of our representations, the speed reduction is shown solely as a difference between r_1 and r_2. All friction related to the speed reduction is applied to θ_1 and corresponds to B_1. The inertia of the speed reduction is added to the inertia of the motor and corresponds to J_1.

A speed reducer amplifies the motor inertia by the square of the speed reduction; this amplification appears in the relatively large values of J_1. The transmission between θ_2 and the springs has very low friction and no speed reduction. Because the high-frequency behavior of the system is generally handled by the springs, low friction and inertia are most important in this part of the AMASC. The low-frequency behaviors of the system are handled by the motor, and thus, friction and inertia can be overcome by relatively low-bandwidth software compensation.

Perhaps the most important aspect of the AMASC, along with the series spring, remotely located motors, and zero-backlash cable drive, is the physically variable series compliance. As stated in Section II, physical compliance is crucial for a running gait, while varying the compliance is a useful control strategy. The AMASC's physical compliance resides in unidirectional fiberglass plates, which have a relatively high energy capacity on the order of 1000 J/kg.

Varying the stiffness of the AMASC is achieved in much the same way as in animals, with cocontraction of opposing nonlinear springs. In the case of animals, the nonlinear spring is the muscle/tendon combination; in the case of the AMASC, the nonlinear spring is formed by a fiberglass plate spring in series with a set of spiral pulleys. The reduction ratio of the pulleys varies proportionally with the fiberglass spring deflection, to create some output spring function, such as $F_z(z) = Kz^2$. Placing two such spring functions in direct opposition results in a single effective spring-force function F_{eff}. The resulting effective spring force is calculated by substituting $(x_3 + \Delta x)$ and $(x_3 - \Delta x)$ for z, where x_3 represents the pretension on the two nonlinear springs, and Δx represents the deflection from their rest position $(x_2 - x_1)$. Combining the two forces results in

$$F_{\text{eff}}(x_3, \Delta x) = F_z(x_3 + \Delta x) - F_z(x_3 - \Delta x). \tag{1}$$

For the simple example of quadratic springs, $F_z(z) = Kz^2$

$$\begin{aligned} F_{\text{eff}} &= K(x_3 + \Delta x)^2 - K(x_3 - \Delta x)^2 \\ F_{\text{eff}} &= 4Kx_3(\Delta x). \end{aligned} \tag{2}$$

In this manner, the stiffness of the resulting system can be changed by adjusting the pretension x_3. Note that the pretension affects the force as much as the displacement Δx. The effective spring force F_{eff} is linear with respect to displacement (in this specific case), but its stiffness is now adjustable. In practice, the rate at which this parameter can be varied depends on the actuator and transmission used. Our prototype is intended for relatively slow changes at low force, such as during the flight phase of a running gait.

The pulley function, $G(z)$, is a design freedom and can be changed to impart a nearly arbitrary function to the spring/pulley system, $F_z(z)$. Logarithmic spiral pulleys were initially chosen because the spring function of the bending fiberglass plates was unknown, because the desired spring function was unknown, and because two logarithmic spirals mesh correctly and provide the desired stiffening function [43]. Our logarithmic spiral pulleys, as diagrammed in Fig. 6, are described by the following

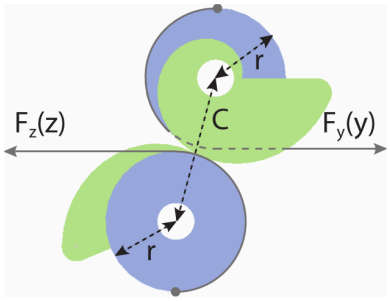

Fig. 6. Logarithmic spiral pulleys used on the prototype AMASC. The spirals roll on each other as if they were gears, and the gray lines ending in arrows show the cables wrapped around the round portion of each pulley. $F_y(y)$ is the force from the fiberglass spring, and $F_z(z)$ is the output-force function from the pulleys.

TABLE II
MEASUREMENTS OF THE LOGARITHMIC SPIRAL PULLEYS

variable	value	description
C	$0.1m$	center distance between axles
r	$0.05m$	radius of the round pulley
k	0.2446489	affects the "steepness" of the spiral
A	0.017696	scales the overall size of the spiral
ϕ_0	-10.2°	position of pulley when $z = 0$

equations (see Table II):

$$R_1 = Ae^{k\phi}$$
$$R_2 = C - Ae^{k\phi}$$

where R_1 and R_2 are the radii of the pulleys at a particular angle of rotation, ϕ, and

$$\phi(z) = \frac{z}{r}. \tag{3}$$

These pulleys exhibit the velocity transfer function

$$\frac{dy}{dz} = \frac{dG}{dz}(z) = \frac{Ae^{kz/r}}{C - Ae^{kz/r}}, \tag{4}$$

and exhibit the position function

$$y = G(z) = r\left(\phi_0 - \frac{1}{k}\ln\left(C - Ae^{kz/r}\right)\right). \tag{5}$$

The choice of a logarithmic spiral was somewhat arbitrary but serves the purposes of this prototype. When designing new pulleys for future implementations, two functions must be considered: the desired output spring-force function $F_z(z)$ and the measured spring-force function $F_y(y)$. The desired spring-force function $F_z(z)$ can be described in terms of the pulley-transmission function $y = G(z)$. We calculate $F_z(z)$ by computing the virtual work:

$$F_z(z)dz = F_y(y)dy$$
$$y = G(z), \qquad dy = \frac{dG}{dz}(z)dz$$
$$F_z(z) = F_y\left(G(z)\right)\frac{dG}{dz}(z). \tag{6}$$

Given the desired F_z and the spring function F_y, we can solve (6) for the pulley function $G(z)$. With this pulley function, the relationship between angular velocities of two members $dG/dz(z)$ can be determined. Given the center distance C between the pulleys, the polar equations describing the spiral shape of both pulleys are

$$R_1 = \frac{C(dG/dz)(z)}{1 + dG/dz(z)}$$
$$R_2 = C - R_1.$$

Even if the fiberglass springs have some unusual stiffness function $F_y(y)$, the spiral pulley function $G_z(z)$ can accommodate the nonlinearity and create almost any desired joint-stiffness function.

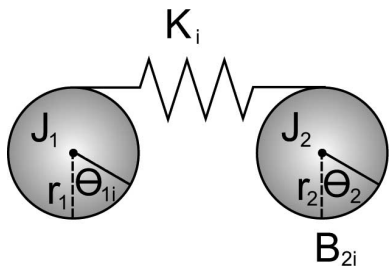

Fig. 7. Ideal case of the AMASC, with three parameters: spring set point θ_{1i}, spring stiffness K_i, and knee-joint damping B_{2i}.

B. Control System Design

The control system is designed for the mechanical model shown in Fig. 4 and is intended to accomplish two basic tasks. The first task is to adjust the mechanism configuration so that its physical properties match the commanded spring stiffness. This adjustment is accomplished with a proportional–integral–differential (PID) position controller and a spring-cancelation feed-forward torque on the pretension motor, x_3. Because the specific position of this motor corresponds to a specific effective stiffness K_{eff}, no further control is required.

The second task is to actively control the motor position, i.e., θ_1, so that the force applied by the pair of springs, i.e., F_{eff}, on θ_2 matches the spring force that would be created by the ideal, correctly tuned system. This ideally tuned system is shown in Fig. 7, with ideal leg stiffness K_i and ideal set point θ_{1i}. When the physical stiffness K_{eff} matches the ideal stiffness K_i, then the motor position θ_1 will be commanded to match the ideal system's set point θ_{1i}. When K_{eff} does not match K_i, then θ_1 must move in some additional corrective trajectory.

The desired motor position θ_1^* is calculated by setting the torque applied by the actual springs on the pulley to match the spring torque of the ideal system

$$K_{\text{eff}}(\Delta x)r_2 + B_2\dot{\theta}_2 = (\theta_2 r_2 - \theta_{1i}r_1)K_i r_2 + B_{2i}\dot{\theta}_2. \tag{7}$$

Assuming quadratic springs as in (2), where $K_{\text{eff}} = 4Kx_3$, and $\Delta x = (x_2 - x_1) = (\theta_2 r_2 - \theta_1 r_1)$, we can solve this equation for θ_1 to calculate the desired position, i.e., θ_1^*, and its derivative $\dot{\theta}_1^*$

$$\theta_1^* = \frac{K_i}{K_{\text{eff}}\,r_1}(\theta_{1i}r_2 - \theta_2 r_2) - \frac{B_{2i} - B_2}{K_{\text{eff}}\,r_1 r_2}\dot{\theta}_2 + \theta_2\frac{r_2}{r_1} \tag{8}$$

$$\dot{\theta}_1^* = -\frac{K_i}{K_{\text{eff}} r_1}\dot{\theta}_2 r_2 - \frac{K_i}{K_{\text{eff}}^2}\dot{K}_{\text{eff}}(\theta_{1i} r_2 - \theta_2 r_2) - \frac{B_{2i} - B_2}{K_{\text{eff}} r_1 r_2}\ddot{\theta}_2 + \frac{B_{2i} - B_2}{K_{\text{eff}}^2 r_1 r_2}\dot{K}_{\text{eff}}\dot{\theta}_2 + \dot{\theta}_2\frac{r_2}{r_1}. \quad (9)$$

Note that when the mechanism matches the desired system (i.e., $K_i = K_{\text{eff}}$, and $B_{2i} = B_2$), the above equations reduce to $\theta_1^* = \theta_{1i}$ and $\dot{\theta}_1^* = 0$.

We then apply a proportional–differential (PD) controller on θ_1 to move it to the desired position, along with a spring cancelation force to hold it against the force applied by the springs (see Fig 8):

$$\tau_{\text{motor}} = K_P(\theta_1^* - \theta_1) + K_D(\dot{\theta}_1^* - \dot{\theta}_1) - F_{\text{eff}}(x_3, \Delta x) r_1. \quad (10)$$

With the spring cancelation force, the PD control can adjust θ_1 as if it were an independent inertia, without the attached spring and associated dynamics. There are two limitations in this approach that introduce error. First, because F_{eff} is a function composed of the logarithmic spiral pulleys and the unknown fiberglass spring function, it is necessarily an approximation. We used a linear approximation of the knee spring, i.e., $F_{\text{eff}} = K_{\text{eff}}\Delta x$, thereby introducing error between the calculated force and the applied force, which is most pronounced at the extremes of deflection and pretension. In addition, when using active control to implement a spring stiffness that is outside the physical range of the AMASC, the calculated location θ_1^* will only be correct to the accuracy of the approximation.

The second source of error comes from the bandwidth limitation on θ_1. When trying to simulate a stiffness at high frequency, the inertia of the motor J_1 will limit its acceleration, and the system will revert to the behavior of its natural dynamics, instead of the desired behavior. However, because the stiffness of the AMASC is adjustable, this error can only happen when the desired stiffness is outside the range of the mechanism, or when the mechanism is in the process of adjusting to the correct stiffness.

IV. Simulation, Results, and Comparison

This section describes the methods and approaches that are used to characterize the physical properties of the AMASC and to build an accurate simulation. All experiments were carried out on the bench top, using batteries for motor power and a small PC104 computer for control. After illustrating the correspondence of the simulation to the real actuator, we demonstrate a simulated running robot and compare its performance using both ideal actuation and our simulated AMASC.

A. Static Compliance Characterization

The first property of the AMASC that we modeled was the static force function of the fiberglass springs and their interaction at the knee, so the control system and the simulation can accurately calculate spring forces as a function of deflection. To gather data on F_{eff} (see Fig. 9), we applied a series of spring set point and pretension values, recorded the motor and leg positions, and measured the force applied by the leg using a load cell. We then applied several different curve-fitting methods to create a representation of the data in which applied force is a function of spring pretension and spring set point.

As can be seen in Fig. 10, the AMASC spring function becomes stiffer at increasing levels of pretension, thereby adjusting its stiffness by a factor of 7 from approximately 2500 to

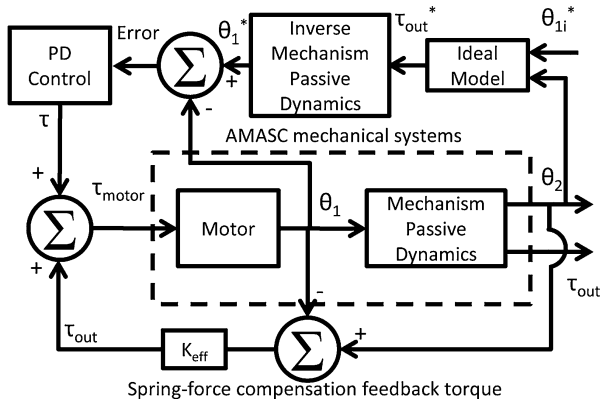

Fig. 8. Block diagram of AMASC hardware and software control system. It is essentially a PD position controller on the AMASC motor, with some methods to calculate the desired position.

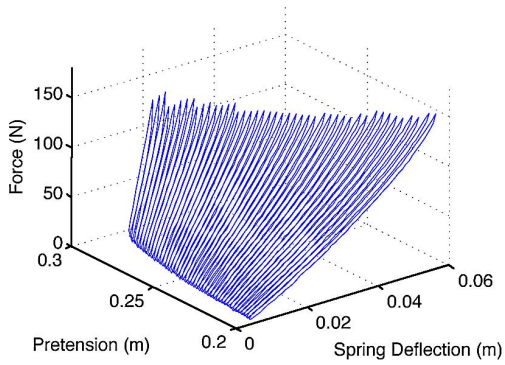

Fig. 9. Three-dimensional plot of spring-function data. Pretension units are in local coordinates of the pretension motor, while the spring deflection units are local to the springs; there is a speed reduction between them. Force is measured from a load cell, which the AMASC leg presses against.

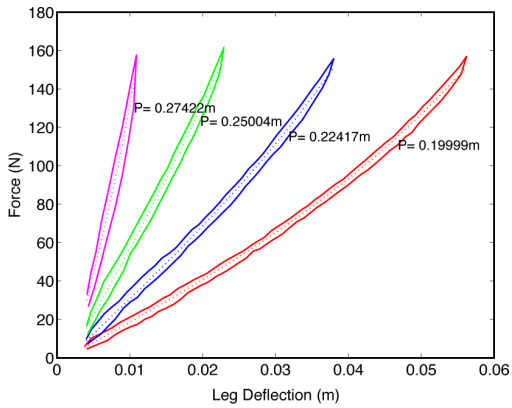

Fig. 10. Spring force response curves at four different pretension, or cocontraction, settings. Each data-based curve has a corresponding analytical curve fit, which is shown as a dotted line.

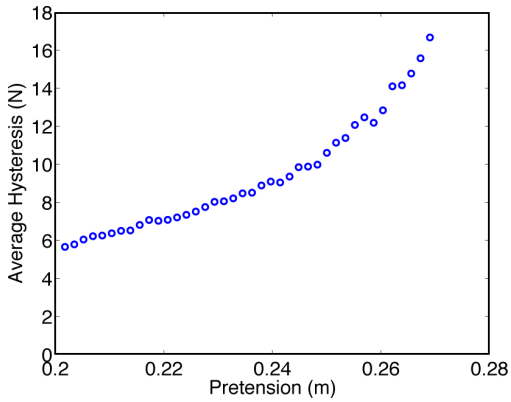

Fig. 11. Hysteresis in the knee due to friction as a function of pretension.

TABLE III
PHYSICAL PROPERTIES USED FOR SIMULATION

variable	value	variable	value
J_1	0.00134 kg·m^2	$M_1 = \frac{J_2}{r_2^2}$	59.6 kg
J_2	0.085 kg·m^2	$M_2 = \frac{J_1}{r_1^2}$	8.5 kg
B_1	0.0517 N·m·s/rad	r_1	0.00474 m
B_2	0.38 N·m·s/rad	r_2	0.1 m

18 000 N/m. The spring function is not exactly linear in deflection, although this can be remedied through pulley design, as discussed in Section III-A. It is also apparent in Fig. 10 that there is some hysteresis due to mechanical friction. This friction increases with increasing tension (and higher bearing forces) in the system, as seen in Fig. 11.

B. Dynamic Actuator Simulation

Dynamic simulation of the AMASC mechanism was done using SD/FAST (a trademark of Symbolic Dynamics, Inc., and Parametric Technology Corporation), based on the model shown in Fig. 4. The springs are approximated as linear springs passed through the logarithmic spiral pulleys, closely matching the measured data. The dynamics of the pretension motor are approximated by a constant velocity trajectory to the desired setting. Physical parameters, such as link length and inertia, were measured from the SolidWorks model and from the AMASC prototype, while the damping ratios were estimated using a binary-search method. The values of these parameters are given in Table III.

We initially compared the prototype AMASC with its simulation by applying a step position input to the set point of both systems. Fig. 12 shows that the responses are very similar. One difference is that the oscillations of the prototype AMASC are damped once the amplitude of the oscillations becomes small. We hypothesize that this is due to frictional effects that are not accurately modeled by the viscous damping included in the model.

For a more comprehensive comparison, we tested the prototype and simulated AMASC across a range of frequencies and stiffness values. Fig. 13 shows the similar responses of the prototype and simulation as the commanded motor position follows

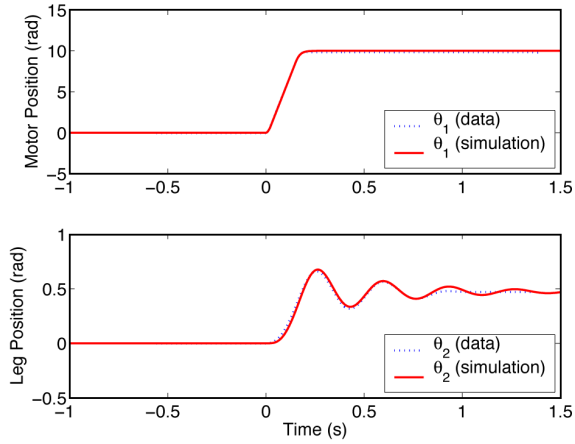

Fig. 12. Comparison of prototype AMASC and simulated AMASC, which shows the close correlation between motor and leg-dynamic response to a step input.

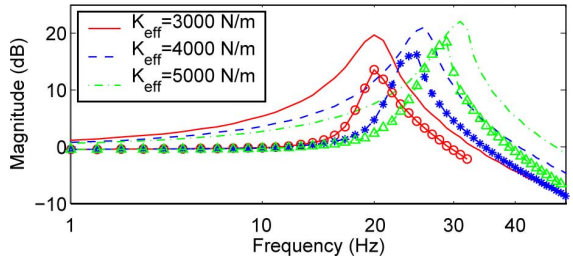

Fig. 13. Behavior of the prototype AMASC and simulated AMASC show close correlation across a range of frequencies at three different stiffnesses. Actuator data are plotted as symbols connected by lines and simulation data are plotted as lines.

a sine-wave function through a range of frequencies at a series of ascending pretension values. We hypothesize again that differences in the simulation and prototype are mostly caused by unmodeled frictional effects, such as stiction on the fiberglass springs, or the change in friction as a function of pretension. Part of the error may also be caused by our spring fit; it has some error and is not an exact representation of the physical system.

These tests do not demonstrate the performance of the AMASC system, they merely show that the physical AMASC and simulated AMASC behave similarly at a range of frequencies. To measure the performance of any actuator, experiments should test how well it demonstrates desired dynamics under various conditions.

The AMASC concept is designed to implement SLIP-model running in the real world, including the ability to vary stiffness and easily handle ground impacts. Impacts imply that this spring-like behavior must exist to an arbitrarily high frequency, which is not possible for a standard gearmotor system. As shown in Fig. 14, the AMASC has no meaningful bandwidth limitations when properly tuned, because the physical system matches the desired spring-like behavior. The Bode plot shows the ratio of the measured versus the commanded spring force, as the leg follows a sine-wave-position trajectory. The three different plots represent three different ideal model stiffness values K_i, with a constant physical stiffness K_{eff}. These plots show the frequency limit of the AMASC when attempting to simulate a

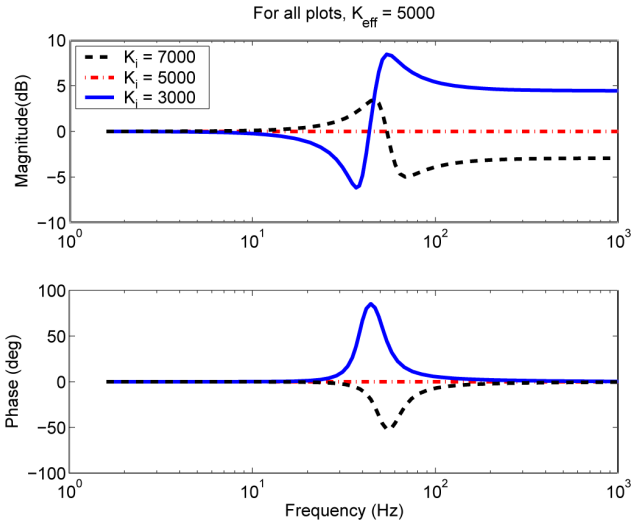

Fig. 14. In this simulation of the AMASC model from Fig. 4, with a constant physical stiffness of $K_{\text{eff}} = 5000$ N/m, three different actively controlled stiffness values are tested by displacing the end effector J_2 at increasing sine wave frequencies and measuring the resulting forces applied on J_2 by the massless springs. The system cannot keep up at high frequencies when the physical stiffness and controlled stiffness do not match, but it has no bandwidth limit when they do.

system softer or stiffer than its mechanical adjustment, as well as demonstrate the lack of a bandwidth limit when the AMASC is tuned properly.

C. Running Simulation

We implemented a simulated running robot in SD/FAST based on the SLIP model to compare with a simulated AMASC runner. Raibert-style controllers were implemented, as described in [34], with slight modifications. Raibert-style hopping-height controllers insert a fixed amount of energy by changing the set point during stance, thus causing the hopping height to converge to some value. Our modification calculates exactly how much energy must be added for the desired hopping height and speed and adjusts the set point to add the appropriate amount of energy.

We first created the running simulation with an ideal actuator placed at each joint, such that we could apply any stiffness and set point instantly. We then converted the actuator in this running simulation to the simulation of the AMASC (see Fig. 15), as described in Section IV-B. The bench-top prototype has relatively soft springs; therefore, the simulated AMASC fiberglass springs, which are represented by Y_A and Y_B, were increased by approximately a factor of 10 over the bench-top prototype to values more appropriate for a running gait. With the stiffer "physical" springs in the running simulation, we could reach the commanded mechanical stiffness.

With the simulated AMASC in place of the ideal actuator, the simulated robot continued to successfully run, with no changes to the running controller. The resulting difference in the behavior of the running robot is shown in Fig. 16. Note that the hopping height and stride length decrease slightly. This change is due to the fact that the set point of the AMASC cannot change instantly,

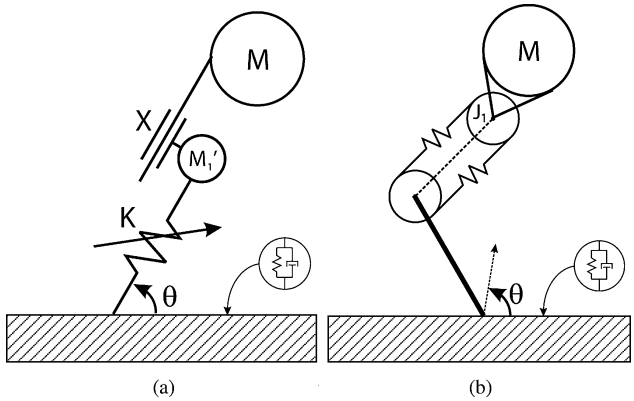

Fig. 15. Hopping robot with the AMASC inserted as the knee spring, compared with the standard SLIP model with reflected motor inertia. The force vector at the toe points toward the hip joint, which is aligned with the effective SLIP-model prismatic spring. (a) SLIP model with reflected motor inertia M_1'. (b) Mathematically equivalent SLIP model with AMASC.

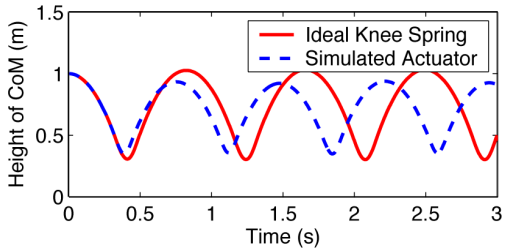

Fig. 16. Comparison of hopping robot behavior with an ideal knee spring and a simulation of the AMASC as the knee spring.

and thus, slightly less energy is inserted into the running gait with our simple PD control than with an ideal knee spring.

V. Discussion

We designed the AMASC as a prototype for running robots; however, it is also a useful concept for other manipulation tasks. In this section, we compare the AMASC and the MIT-SEA, discuss limitations and drawbacks of the AMASC, and offer some conclusions and the direction of future work on this subject.

A. Massachusetts Institute of Technology Series Elastic Actuator Comparison

Although the AMASC is designed to match the desired natural dynamics for a particular SLIP-model running gait, it can be operated as a force-controlled actuator by disabling the variable stiffness and implementing an appropriate software controller. With this modification, the AMASC has the exact same mechanical model as the MIT-SEA but with much lower physical stiffness, about half the dynamic mass and, most importantly, orders of magnitude greater energy storage capacity [19]. The performance characteristics are comparable with the MIT-SEA.

B. Advantages of the Actuator With Mechanically Adjustable Series Compliance as a Manipulator

A major advantage of the AMASC over other variable-stiffness mechanisms is the small, braked motor to vary and

hold pretension. The spring set-point motor does not see any forces from changes in joint stiffness. Many existing mechanisms use antagonistic motor pairs, which must exert forces both to precompress the springs and to move the joint, and thus, the required motor size and mass for such an antagonistic system are much larger than the AMASC [25], [27]–[32], [44].

The cable-drive design of the AMASC allows for very low mass at the actuated joint, because the electric motors and other heavy components can be placed near the base of the robot. The structure and springs placed at the joint have relatively low mass, and because the springs are used both for energy storage and force sensing, the performance of the AMASC does not suffer due to friction or stretch in a long cable transmission.

Finally, the passive stiffness of the joint is a design freedom of this device, due to nonlinear pulleys in the cable transmission. They can be machined to create nearly any joint stiffness function, and this can be important to create a model-based mechanism.

C. Limitations and Drawbacks

One difference between variable compliance designs for manipulation and designs for legged locomotion is the energy-storage requirement. For locomotion, it is important to have springs that are large enough to store the energy of a running gait. For manipulation tasks, little or no energy is stored—the physical compliance is mainly for safety or control system stability.

While the AMASC was designed with large springs for a running gait, the physically variable compliance comes at a cost in mass and complexity. There are several effects that can significantly reduce the energy storage capacity of antagonistic springs over a single, nonadjustable spring of the same size. First, only one of the springs is actually compressing when the joint compresses, thereby halving the potential energy storage. The other spring is actually relaxing and releasing its energy into the compressing spring rather than into the joint. Additionally, the individual spring deflections are the sum of both the cocontraction and the joint deflection. Assuming there is an upper and lower limit on the spring deflection, increasing the cocontraction will reduce the maximum allowable joint deflection. If the joint stiffness is to be adjusted by a factor of three (for example), then the maximum joint deflection will be significantly reduced, and the combined effects reduce the energy density of the springs for this example to $(\frac{1}{2} \times \frac{6}{7} \times \frac{1}{3}) = \frac{1}{7}$ of a nonadjustable spring.

Aside from the reduction in energy storage capacity, using antagonistic pairs of springs increases internal forces beyond the applied joint forces, which increases friction and requires stronger parts. There is also an extra actuator for stiffness adjustment and other additional parts when compared with a nonadjustable system, which add mass and complexity. These disadvantages can be overcome, but should be considered when creating new robot designs based on the ideas demonstrated by the AMASC.

During the construction and experimentation of the AMASC, we discovered a few practical considerations in the mechanical design. For example, the block-and-tackle system suspends pulleys in the middle of a length of cable—and this suspended mass can oscillate uncontrollably during certain frequency tests. It did not affect our experiments but would be a drawback in a real system that might have regular impacts with the ground to excite this oscillation. Another practical consideration is the size of the springs. They are as large as can fit on the AMASC, but would need to be much larger to store energy for a running robot. The concept is sound, but future designs will take into account these practical considerations.

VI. Conclusion and Future Work

Physical compliance and mechanical energy storage are crucial for a successful running gait, while variable compliance is a useful control parameter for SLIP-model running or manipulation tasks. The AMASC uses a novel combination of a cable-drive transmission, cable differential, series springs, and spiral-shaped pulleys to store mechanical energy and allow tunable compliance with an engineered spring function. In addition, it has very low friction and zero backlash. Within its range of mechanical compliance adjustment, the AMASC has virtually no bandwidth limitations for the task of spring-like behavior and is similar to an ideal SLIP. Due to this relation, a robot based on the concepts demonstrated by the AMASC could be controlled using the simple SLIP model as a template while ignoring most of the complex mechanism details.

It has been said that running is merely a robot juggling itself, thereby implying a close relationship between legged locomotion and manipulation tasks. Indeed, the AMASC concept and its variable stiffness is ideal for force-controlled manipulation tasks. There is a tradeoff between stiffness and performance for many tasks, and it is beneficial to adjust the stiffness many times during a particular set of motions. As part of our future work, we plan to characterize and quantify the relationship between series impedance and bandwidth limitations for carefully defined tasks, such as applying a constant force against a moving object or damping an impact. Through the investigation of fundamental actuation principles in theory, in simulation, and through proof-of-concept implementation, we hope to provide guidelines for the design and implementation of actuators that are optimized for a particular task. Designers of large, complex systems, such as running robots and robotic exoskeletons, will be able to build on this work.

References

[1] W. J. Schwind and D. E. Koditschek, "Characterization of monopod equilibrium gaits," in *Proc. IEEE Int. Conf. Robot. Autom.*, Apr. 1997, pp. 1986–1992.

[2] R. Blickhan, "The spring-mass model for running and hopping," *J. Biomech.*, vol. 22, no. 11/12, pp. 1217–1227, 1989.

[3] T. A. McMahon and G. C. Cheng, "The mechanics of running: How does stiffness couple with speed?" *J. Biomech.*, vol. 23, pp. 65–78, 1990.

[4] K. Kemper, D. Koepl, and J. Hurst, "Optimal passive dynamics for torque/force control," presented at the Int. Conf. Robot. Autom., Anchorage, AK, 2010.

[5] J. W. Hurst, J. E. Chestnutt, and A. A. Rizzi, "An actuator with physically adjustable compliance for highly dynamic legged locomotion," in *Proc. IEEE Int. Conf. Robot. Autom.*, 2004, pp. 4662–4667.

[6] R. J. Full and C. T. Farley, "Musculoskeletal dynamics in rhythmic systems—A comparative approach to legged locomotion," in *Biomechanics and Neural Control of Posture and Movement*, J. M. Winters and P. E. Crago, Eds. New York: Springer-Verlag, 2000.
[7] R. Blickhan and R. J. Full, "Similarity in multilegged locomotion: Bouncing like a monopode," *J. Comp. Physiol.*, vol. 173, pp. 509–517, 1993.
[8] J. R. Hutchinson, D. Famini, R. Lair, and R. Kram, "Are fast-moving elephants really running?" *Nature*, vol. 422, pp. 493–494, 2003.
[9] Honda Corp. Asimo humanoid robot [Online]. Available: http://world.honda.com/ASIMO/
[10] G. A. Cavagna, "Elastic bounce of the body," *J. Appl. Physiol.*, vol. 29, no. 3, pp. 279–282, 1970.
[11] T. A. McMahon, "Mechanics of locomotion," *Int. J. Robot. Res.*, vol. 3, no. 2, pp. 4–28, 1984.
[12] D. P. Ferris and C. T. Farley, "Interaction of leg stiffness and surface stiffness during human hopping," *Amer. Physiol. Soc.*, vol. 82, pp. 15–22, 1997.
[13] C. T. Farley, H. H. P. Houdijk, C. V. Strien, and M. Louie, "Mechanism of leg stiffness adjustment for hopping on surfaces of different stiffnesses," *Amer. Physiol. Soc.*, vol. 85, pp. 1044–1055, 1998.
[14] T. A. McMahon, "The role of compliance in mammalian running gaits," *J. Exp. Biol.*, vol. 115, pp. 263–282, 1985.
[15] J. K. Hodgins and M. H. Raibert, "Adjusting step length for rough terrain," *IEEE Trans. Robot. Autom.*, vol. 7, no. 3, pp. 289–298, Jul. 1991.
[16] D. P. Ferris, M. Louie, and C. T. Farley, "Running in the real world: Adjusting leg stiffness for different surfaces," in *Proc. Roy. Soc. London*, Jan. 1998, vol. 265, pp. 989–993.
[17] C. T. Farley and O. Gonzalez, "Leg stiffness and stride frequency in human running," *J. Biomech.*, vol. 29, no. 2, pp. 181–186, 1996.
[18] C. T. Farley, J. Glasheen, and T. A. McMahon, "Running springs: Speed and animal size," *J. Exp. Biol.*, vol. 185, pp. 71–87, 1993.
[19] D. W. Robinson, "Design and analysis of series elasticity in closed-loop actuator force control," Ph.D. dissertation, Mass. Inst. Technol., Cambridge, MA, Jun. 2000.
[20] J. Pratt, P. Dilworth, and G. Pratt, "Virtual model control of a bipedal walking robot," in *Proc. Int. Conf. Robot. Autom.*, 1997, pp. 193–198.
[21] J. Pratt and G. Pratt, "Exploiting natural dynamics in the control of a planar bipedal walking robot," in *Proc. 36th Annu. Allerton Conf. Commun., Control, Comput.*, Sep. 1998, pp. 739–748.
[22] D. J. Paluska, "Design of a humanoid biped for walking research," Master's thesis, Mass. Inst. Technol., Cambridge, MA, 2000.
[23] J. Pratt, C.-M. Chew, A. Torres, P. Dilworth, and G. Pratt, "Virtual model control: An intuitive approach for bipedal locomotion," *Int. J. Robot. Res.*, vol. 20, pp. 129–143, 2001.
[24] B. Vanderborght, R. V. Ham, D. Lefeber, T. G. Sugar, and K. W. Hollander, "Comparison of mechanical design and energy consumption of adaptable, passive-compliant actuators," *Int. J. Robot. Res.*, vol. 28, pp. 90–103, 2009.
[25] K. F. Laurin-Kovitz, J. E. Colgate, and S. D. R. Carnes, "Design of components for programmable passive impedance," in *Proc. IEEE Int. Conf. Robot. Autom.*, Apr. 1991, pp. 1476–1481.
[26] D. R. Nahar and T. Sugar, "Compliant constant-force mechanism with a variable output for micro/macro applications," in *Proc. IEEE Int. Conf. Robot. Autom.*, 2003, pp. 318–323.
[27] T. Morita and S. Sugano, "Design and development of a new robot joint using a mechanical impedance adjuster," in *Proc. IEEE Int. Conf. Robot. Autom.*, 1995, pp. 2469–2475.
[28] A. Bicchi, G. Tonietti, M. Bavaro, and M. Piccigallo, "Variable stiffness actuators for fast and safe motion control," presented at the Int. Symp. Robot. Res., Siena, Italy, 2003.
[29] A. Bicchi and G. Tonietti, "Fast and "soft-arm" tactics," *IEEE Robot. Autom. Mag.*, vol. 11, no. 2, pp. 22–33, Jun. 2004.
[30] S. A. Migliore, E. A. Brown, and S. P. DeWeerth, "Biologically inspired joint stiffness control," in *Proc. IEEE Int. Conf. Robot. Autom.*, 2005, pp. 4508–4513.
[31] K. Koganezawa, T. Inaba, and T. Nakazawa, "Stiffness and angle control of antagonistically driven joint," presented at the IEEE/RAS-EMBS Int. Conf. Biomed. Robot. Biomechatronics, Pisa, Italy, 2006.
[32] N. Vitiello, T. Lenzi, J. McIntyre, S. Roccella, E. Cattin, F. Vecchi, and M. C. Carrozza, "Characterization of the neurarm bio-inspired joint position and stiffness open loop controller," in *Proc. IEEE/RAS-EMBS Int. Conf. Biomed. Robot. Biomechatronics*, Oct. 2008, pp. 138–143.
[33] R. V. Ham, B. Vanderborght, B. Verrelst, M. V. Damme, and D. Lefeber, "MACCEPA: The mechanically adjustable compliance and controllable equilibrium position actuator used in the controlled passive walking biped veronica," in *Proc. 15th Int. Symp. Meas. Control Robot.*, Houston, TX, 2005.
[34] M. Raibert, *Legged Robots That Balance*. Cambridge, MA: MIT, 1986.
[35] A. N. S. H. Koh Hosoda and T. Takuma, "Biped robot design powered by antagonistic pneumatic actuators for multi-modal locomotion," *Robot. Auton. Syst.*, vol. 56, pp. 46–53, 2008.
[36] J. D. Schutter, "A study of active compliant motion control methods for rigid manipulators based on a generic control scheme," in *Proc. IEEE Int. Conf. Robot. Autom.*, 1987, pp. 1060–1065.
[37] S. D. Eppinger and W. P. Seering, "Understanding bandwidth limitations in robot force control," in *Proc. IEEE Int. Conf. Robot. Autom.*, 1987, pp. 904–909.
[38] D. A. Lawrence, "Actuator limitations on achievable manipulator impedance," in *Proc. IEEE Int. Conf. Robot. Autom.*, 1989, pp. 560–565.
[39] Y. Matsuoka and R. D. Howe, "Hand impedance change during learning of a novel contact task," in *Proc. World Congr. Med. Phys. Biomed. Eng.*, Chicago, IL, 2000.
[40] D. J. Bennett, "What are the advantages of variable stiffness control?" in *Proc. IEEE Eng. Med. Biol.*, Dec. 1992, pp. 86–87.
[41] E. Burdet, R. Osu, D. W. Franklin, T. E. Milner, and M. Kawato, "The central nervous system stabilizes unstable dynamics by learning optimal impedance," *Nature*, vol. 414, pp. 446–449, Nov. 2001.
[42] W. T. Townsend and J. K. Salisbury, "Mechanical bandwidth as a guideline to high-performance manipulator design," in *Proc. IEEE Int. Conf. Robot. Autom.*, 1989, vol. 3, pp. 1390–1395.
[43] N. P. Chironis, "Types of noncircular gears," in *Mechanisms, Linkages, and Mechanical Controls*. New York: McGraw-Hill, 1965, pp. 241–244.
[44] J. K. Mills, "Hybrid actuator for robot manipulators: Design, control and performance," in *Proc. IEEE Int. Conf. Robot. Autom.*, 1990, pp. 1872–1878.

Jonathan W. Hurst received the B.S. degree in mechanical engineering, the M.S. degree in robotics, and the Ph.D. degree in robotics from Carnegie Mellon University, Pittsburgh, PA, in 2001, 2004, and 2008, respectively.

He is currently an Assistant Professor of mechanical engineering with Oregon State University, Corvallis. His research interests include legged locomotion, natural dynamics, and robot actuation.

Joel E. Chestnutt received the M.S. and Ph.D. degrees from the Robotics Institute, Carnegie Mellon University, Pittsburgh, PA, in 2006 and 2007, respectively.

He is currently a Postdoctoral Researcher with the Digital Human Research Center, National Institute of Advanced Industrial Science and Technology, Tokyo, Japan. His research interests include legged locomotion, motion planning, and dynamic stability.

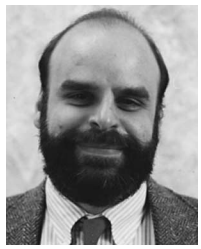

Alfred A. Rizzi received the Sc.B. degree in electrical engineering from the Massachusetts Institute of Technology, Cambridge, in 1986, and the M.S. and Ph.D. degrees from Yale University, New Haven, CT, in 1990 and 1994, respectively.

He is currently the Lead Robotics Scientist at Boston Dynamics, Inc., Boston, MA, where he directs research on novel mobility and locomotion systems. Prior to joining Boston Dynamics, in 2006, he was an Associate Research Professor in the Robotics Institute at Carnegie Mellon University, Pittsburgh, PA, where he directed research projects focused on hybrid sensor-based control of complex and distributed dynamical systems. Highlights of these projects include the development of embedded software systems and automated behaviors for novel legged mobile robots (RiSE and RHex) as well as a modular automated assembly system (Minifactory). He is a member of the Advisory Board of the *International Journal of Robotics Research.*

Dr. Rizzi is a corecipient of the Nakamura Prize for best paper at the International Symposium on Intelligent Robots and Systems in 2001.